ADVANCED MATERIALS
www.advmat.de

Materials Views
www.MaterialsViews.com

# Three-Dimensional Magnetic Assembly of Microscale Hydrogels

*Feng Xu, Chung-an Max Wu, Venkatakrishnan Rengarajan, Thomas Dylan Finley, Hasan Onur Keles, Yuree Sung, Baoqiang Li, Umut Atakan Gurkan, and Utkan Demirci**

Most tissues in organisms are composed of repeating basic cellular structures (i.e., functional units[1]), such as the lobule in the liver and the nephron in kidney, and islets in the pancreas. In vivo, cells in these functional units are embedded in a 3D microenvironment composed of extracellular matrix (ECM) and neighboring cells with a defined spatial distribution. Tissue functionality arises from these components and the relative spatial locations of these components.[1,2] Tissue engineering approaches, therefore, attempt to recreate the native 3D architecture in vitro. The importance of the 3D architecture on actual native tissue function has been reported.[3–7] Control over the 3D architecture enables researchers to define structure-to-function relationships as well as perform theoretical analyses and to model cellular events and diseases.[8–10] Biodegradable scaffolds and other top-down approaches to engineer tissues offer limited control over the 3D architecture to replicate such complex features. Bottom-up methods, which involve assembling microscale building blocks (e.g., cell encapsulating microscale hydrogels) into larger tissue constructs, have the potential to overcome these limitations, since control over the features of individual building blocks (e.g., composition and shape) may be exercised.[11–13]

Although bioreactors for microgel assembly dependent on stirring/agitation, self-assembly,[14] multilayer photopatterning,[15] and hydrophilic–hydrophobic interactions[16] have been developed to allow 3D cellular architecture, such methods have not been broadly available in practical applications.[5,17,18] Since these methods have not been able to show multilayer assembly of microgels with control, these existing assembly approaches to engineer tissues offer limited control over the 3D micro-architecture. For instance, multilayer photopatterning and microfluidic-directed assembly can also be used to create highly sophisticated microgel assembly architectures,[19,20] but long operational times and complex peripheral equipment are usually required. Photopatterning may also suffer from multiple ultraviolet light exposures to create multilayer structures, and this method was mostly used for 2D surface patterning to achieve simple geometries.[21–23] Although the capability to fabricate microscale cell-laden hydrogels using the photopatterning method has been shown, 3D assembly of these microgels to form larger 3D complex constructs is still a challenge. Therefore, a straightforward technology enabling 3D microgel assembly therefore remains an unmet need.[5,18] To address these challenges, we have fabricated magnetic nanoparticle (MNP) loaded cell-encapsulating microscale hydrogels (M-gels) and assembled these gels into 3D multilayer constructs using magnetic fields (**Figure 1** and Figure S1, Supporting Information). By spatially controlling the magnetic field, 3D construct geometry can be manipulated, and multilayer assembly of multiple microgel layers can be achieved.

Magnetics have been exploited in a variety of direct cellular manipulation, cell sorting, 3D cell culture, local hyperthermia therapy, and clinical imaging applications.[10,24–31] Magnetic fields have been utilized to manipulate cells to achieve 3D tissue culture leveraging magnetic levitation.[32] In this method, cells were encapsulated in a bioinorganic hydrogel composed of bacteriophages, magnetic iron oxide, and gold nanoparticles, where the bacteriophage had a ligand peptide targeting the gold nanoparticles and magnetic iron oxide. The incorporation of MNPs has been employed to create 2D surface patterns,[25,33–35] form 3D cell culture arrays,[36] and characterize cell-membrane mechanical properties.[37] In most of these magnetic methods, cells were first mixed directly with a ferrofluid or functionalized MNPs and then exposed to external magnetic fields, allowing for controlled manipulation. In addition, methods to encapsulate MNPs in hydrogel microparticles have been developed based on microfluidics[28,38–40] and applied to multiplexed bioassays.[41,42] However, although MNPs have been adjusted to bind to cells, the combination of MNPs and cell encapsulation in microgels and their magnetic assembly to achieve 3D multilayer constructs has not yet been systematically applied.

To evaluate the manipulation of M-gels by magnetic fields, we developed a magnetic assembler (Figure 1b and Figure S2,

Dr. F. Xu, C.-a. M. Wu, V. Rengarajan, T. D. Finley, H. O. Keles, Y. Sung, Dr. B. Li, Dr. U. A. Gurkan, Dr. U. Demirci
Bio-Acoustic-MEMS in Medicine (BAMM) Laboratory
Center for Biomedical Engineering
Department of Medicine
Brigham and Women's Hospital
Harvard Medical School
Boston, MA, 02115, USA
E-mail: udemirci@rics.bwh.harvard.edu
Dr. U. Demirci
Harvard-MIT Division of Health Sciences and Technology
Massachusetts Institute of Technology
Brigham and Women's Hospital
Harvard Medical School
Cambridge, MA, 02139, USA

DOI: 10.1002/adma.201101962


© 2011 WILEY-VCH Verlag GmbH & Co. KGaA, Weinheim

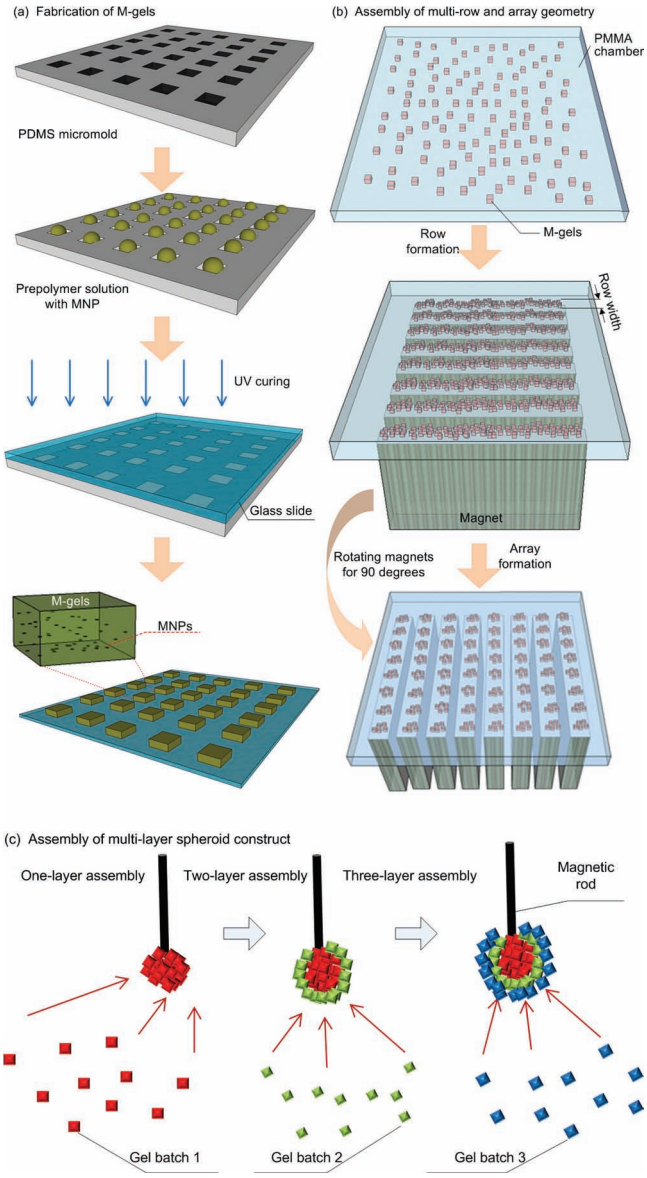


**Figure 1.** Schematic of magnetic directed assembly of microgels. a) M-gels are fabricated by micromolding. b) M-gels in a fluidic chamber are assembled into rows and arrays of constructs. The scattered M-gels are arranged from a random distribution to a row formation by parallel magnets separated by poly(methyl methacrylate) (PMMA) spacers. They are then assembled into an array formation by rotating the magnets by 90 degrees to the base of the chamber. c) M-gels are assembled to fabricate three-layer spheroids through the application of external magnetic fields.

Supporting Information), where M-gels were enclosed in a chamber and subjected to a magnetic field (**Figure 2**a). To test the magnetic response of M-gels, we applied a magnetic field to the chamber using parallel sheet magnets (Figure 1b). The resulting constructs assembled in a line geometry as multiple rows (Figure 2b). To better understand this phenomenon, we performed finite element analysis of the magnetic field patterns in the microgel assembly chamber. The simulation results (Figure 2c) agreed with experimental observations (Figure 2b). For the parallel magnets, the axes of magnetization ran parallel to the chamber surface. The magnetic field strength was greatest immediately adjacent to the magnets while the space between magnets corresponded to local minima in the magnetic field (Figure 2c). This magnetic field led to a parallel, linear chain pattern at the onset of assembly produced by the force that attracts the M-gels towards the field maximum. We observed the assembled constructs to retain their shape and remain intact after the magnets were removed (Figure 2b). Breaks in chains (Figure 2b) were observed when a low number of M-gels were placed into the magnetic assembler (200 gels $mL^{-1}$). The magnetic spacers (poly(methyl methacrylate), PMMA) influence the flux lines between adjacent magnets. The magnetic field is stronger and the gradient is steep in the vicinity of the outer magnets depending on the location and orientation of the magnets. In addition, when the assembly chamber size is larger than the magnet area, gels outside the magnets are drawn primarily to the outer magnetic field zones (Figure 2b). The inner magnetic zones attract gels in their immediate vicinity. Thus, the outer magnets effectively draw gels from a larger chamber volume than the inner magnets based on the chamber design. A high concentration of gels loaded into the chamber minimized the dependency of assembled row width of the constructs on the relative positioning and magnitude of the magnetic flux density maxima and minima.

To tune row width, we assembled microgels using different numbers of magnets placed under the assembly chamber (Figure 1b, and Figure 2b,c). We observed that by reducing the number of magnets and holding the number of gels constant, the same number of gels was distributed among fewer magnetic field maxima (Figure 2b). This gave wider assembled constructs. The average row widths were observed as 1435 ± 113, 877 ± 49, 537 ± 75, 438 ± 33, and 406 ± 67 μm for $n$ = 1, 2, 3, 4, and 5 magnets, respectively (Figure 2d). The row assembly process took less than a second (Video S1, Supporting Information) indicating rapid assembly and potential for scalability. By further rotating the magnets, a microgel array with uniform element size was formed (Figure 1b and Figure S3, Supporting Information), and there was no significant variation in uniformity between arrays of different sizes (Figure S3m, Supporting Information), indicating the scalability of the platform. In addition, the assembly time for array formation by magnetic manipulation of M-gels increased with increasing array size from 2 × 2 to 8 × 8 (Figure S3n, Supporting Information).

Having demonstrated the ability to manipulate M-gels, we subsequently used NIH 3T3 cells as a model to evaluate the magnetic assembly and cell viability after the assembly process steps (**Figure 3**). We observed that cell viability in M-gels over 5 d, and in controls of poly(ethylene glycol) (PEG) without MNPs, were comparable (Figure 3a,b). Within the initial 24 h, the cell viabilities in both MNP M-gels and in controls were above 80%, which reached ~70% and remained at that level at days 3 and 5. The cell viability was observed to decrease over 5 d even in the controls, where no MNPs were encapsulated. These results agreed with earlier reports on cell viability with PEG gels.[43,44] We also tracked the cell growth, attachment, and spread in the M-gels. We observed that the cells grew, attached, and spread within the gels and formed a 3D microtissue construct after 108 h (Figure 3c–g).


© 2011 WILEY-VCH Verlag GmbH & Co. KGaA, Weinheim

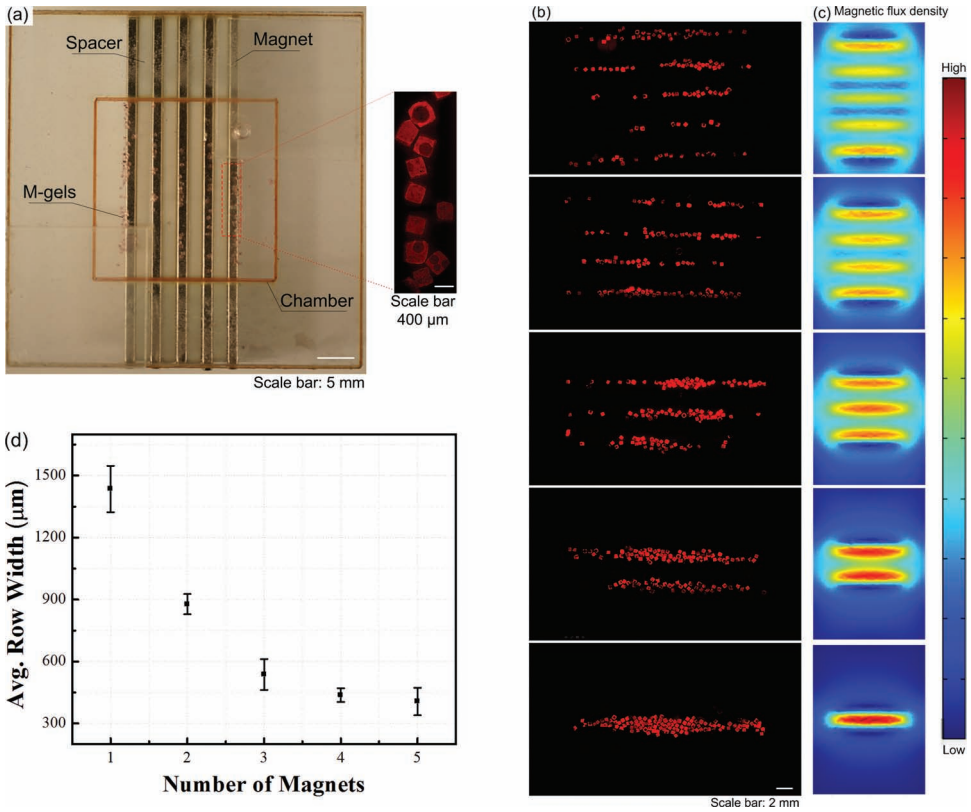


**Figure 2.** Row assembly of M-gels. a) The magnetic assembler. Fluorescence images of microgels assembled in phosphate buffered saline (PBS), b) aligned using 1 to 5 magnets as compared to c) in-channel magnetic flux density simulated using finite element analysis. d) Effect of number of magnets on average assembled row width using the same number of microgels per chamber. Row widths from multiple constructs were averaged to obtain the mean and standard deviation for the process.

The presented approach can also provide temporal and spatial control to manipulate microgels in a 3D environment. To demonstrate this, we fabricated 3D multilayer spherical constructs using the assembly system, in which M-gels were collected onto the tip of a magnetic rod and each layer was stabilized by a second crosslinking using a filling layer of PEG. Using a filling layer between multiple gels may increase the cell–cell distances, with effects on cell–cell communication. Hence, minimal gaps and maximum contact between microgels is advantageous during assembly. On the other hand, the cells in hydrogels are shown to self-assemble and migrate in the hydrogels after culture.[5,45–47] The process took 5 s to assemble a 10 mm diameter 3D single-layer spheroid (Video S2, Supporting Information). By varying the MNP concentration in M-gels, single-layer spheroid assemblies of different sizes were achieved (**Figure 4**a,b). The gaps remaining between microgels after assembly were filled with PEG and crosslinked to stabilize the structure, which eliminated disassembly (Figure 4b). The maximal assembled spheroid diameters were 1.89 ± 0.11, 2.13 ± 0.13, 2.46 ± 0.21, 2.61 ± 0.15, and 3.13 ± 0.11 mm at MNP concentrations of 0.003, 0.005, 0.010, 0.015, and 0.020 g $mL^{-1}$, respectively (Figure 4c). To assess the effect of microgel size on the assembly process, we assembled spheroid constructs using three microgel sizes (200 μm, 400 μm, and 1 mm). We observed that the number of microgels needed to achieve a maximum assembly size for a fixed magnetic field decreased with increasing microgel size (Figure 4d), while the diameter of the assembled structure increased (Figure 4e). Although there was a difference in the assembly time for different microgel sizes (Figure 4f), it took less than 3 s in all the cases. Other complex constructs were also fabricated by combining a magnetic field with flexible surfaces (Figure 4g,h), such as an arc (Figure 4g) and a dome (Figure 4h). These geometries were chosen as examples to mimic structures observed in vivo, e.g., a dome for the diaphragm (dome-shaped muscle) beneath the lungs, a tube for vascular structures, a sphere for islets, and a hexagon for lobules in the pancreas. The capability to control the spheroid size by varying MNP concentration allowed fabrication of 3D multilayer spheroids (Figure 4i–o). Such capability to assemble microgels into complex shapes (e.g., such as spherical, dome, and tube shaped gels) of multilamellar structures brings a unique potential to 3D assembly.

Hydrogels are 3D crosslinked networks of polymers that feature advantageous biological properties, including moldability, high porosity, and diffusion controllability, which resemble the physical characteristics of the native cell microenvironment.[48] We have used two types of hydrogels to create


© 2011 WILEY-VCH Verlag GmbH & Co. KGaA, Weinheim

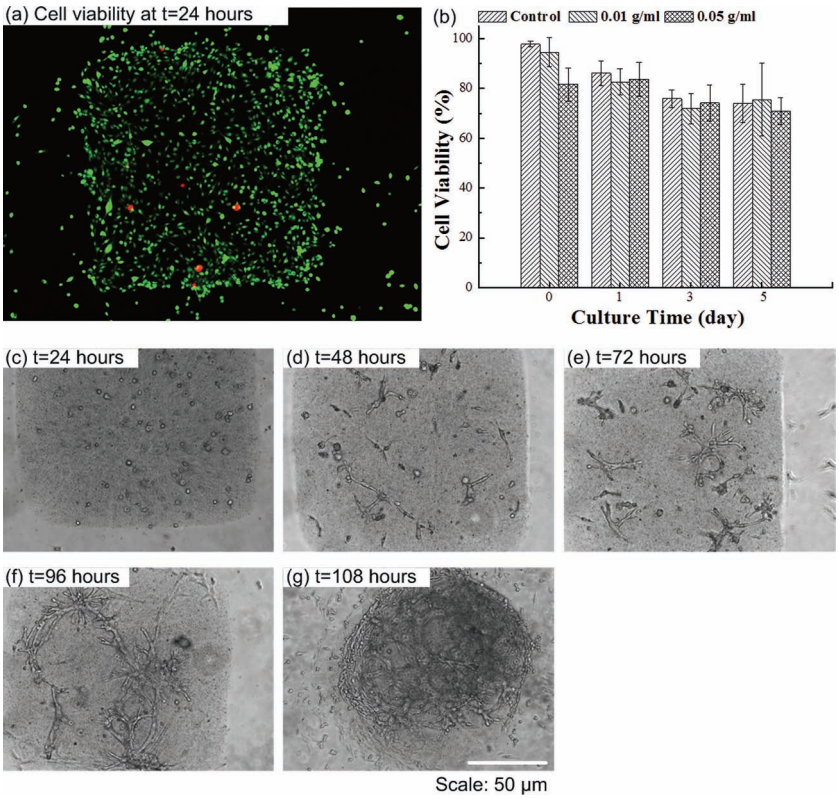


**Figure 3.** Cell encapsulation in M-gels. a) Fluorescent image of live/dead staining of 3T3 cells in M-gels at $t = 24$ h (green represents live cells, red represents dead cells). b) 3T3 cell viability in M-gels was comparable to the controls over a five day culture. The cell viability was normalized to that of controls in a culture flask (97.8%). Cell viability in M-gels for each day was comparable to the microgel controls without MNPs. Images of 3T3 cells in M-gels at c) $t = 24$ d) $t = 48$ e) $t = 72$ f) $t = 96$, and g) $t = 108$ h. The images (c–g) indicated the presence of cells in M-gels, which were observed to attach and spread within the gel as the gel biodegrades over time.

M-gels for the assembly process, i.e., gelatin methacrylate (GelMA) and PEG. GelMA is biodegradable and PEG gels can be modified to become biodegradable. Although PEG is not biodegradable and cells may not come in direct contact with cells from other gels, PEG can be functionalized with functional groups for various applications, such as for controlled differentiation of human mesenchymal stem cells encapsulated in PEG-based hydrogels.[49] The PEG can also be modified to become biodegradable.[50,51] In addition, the magnetic assembly method reported here is not limited to PEG and could be extended to other hydrogels such as agarose, GelMA, and PELGA (poly(methoxyethylene glycol)-*co*-poly(lactic acid)-*co*-poly(glycolic acid)). Since the assembly process is determined by the interaction of the magnetic particles in the M-gel with the magnetic field, we did not observe any differences in the assembly process of the degradable and biodegradable gels. Furthermore, cells are reported to self-assemble and migrate in 3D hydrogels in vitro in various hydrogels such as collagen, matrigel, and fibrinogen.[5,21,45–47,52] These studies not only show that cells can migrate in a 3D hydrogel matrix, but also that the migration behavior in three dimensions is different from that on 2D surfaces.[45] For instance, the maximum migration speed of human prostate carcinoma cells on 2D substrates and 3D substrates are different, and depends on the mechanical properties of the matrix.[46]

The incorporation of MNPs into microgels creates a new biomaterial that maintains the biocompatibility of hydrogels,[53,54] while contributing additional capabilities for cell culture, magnetic manipulation, and complex 3D assembly of microgels. The United States Food and Drug Administration (FDA) has approved the use of MNPs in several applications such as imaging agents,[55] and tolerability of mammalian cells to MNPs has been demonstrated under used conditions.[33,34,56] In addition, MNPs do not need to stay for prolonged times within the assembled constructs and they can be released as the gels biodegrade, and cells secrete their own ECM and take over the space. Therefore, magnetically directed assembly of microgels may become a practical biotechnological tool. Although MNPs are used clinically, further toxicological studies would be beneficial for other types of applications including 3D microgel assembly.

The technology presented here offers an alternative to top-down biodegradable scaffold approaches,[57–59] which face cell seeding limitations because of slow propagation of cells and delayed establishment of cell–cell interactions. On the other hand, MNP-based microgel assembly allows adaptable manipulation of microgels and has the potential to provide an improved 3D architecture and microenvironment for cell growth predetermined by the assembly design and microgel composition. This method is cost-effective, since it does not require specific peripheral equipment, and is compatible with standard cell culture and hydrogel techniques. The magnetic-driven assembly offers several advantages over existing methods including self-assembly. The assembly time by the existing assembly methods are within the order of tens of minutes without considering the time for the chemical manipulation of microgels, where they are exposed to potentially toxic chemicals. In contrast, the magnetic approach is rapid (≈seconds) without these lengthy preprocessing steps and MNPs are regularly mixed as a part of the microgel with cells. In addition, the existing assembly methods provide no control over the 3D assembly process where any microgel can end up being assembled at a specific location. The magnetic field can be extrapolated to assemble microgels with spatial control. Although we have not used focused magnetic fields in this paper to control a single microgel, this technology, in principle, enables high level of control as shown by earlier work on the magnetic control of a nanoneedle in the retina,[60] indicating a significant improvement over the existing assembly methods. Even the directed assembly methods that use hydrophobicity and hydrophilicity[61] do not assemble a single gel with


© 2011 WILEY-VCH Verlag GmbH & Co. KGaA, Weinheim

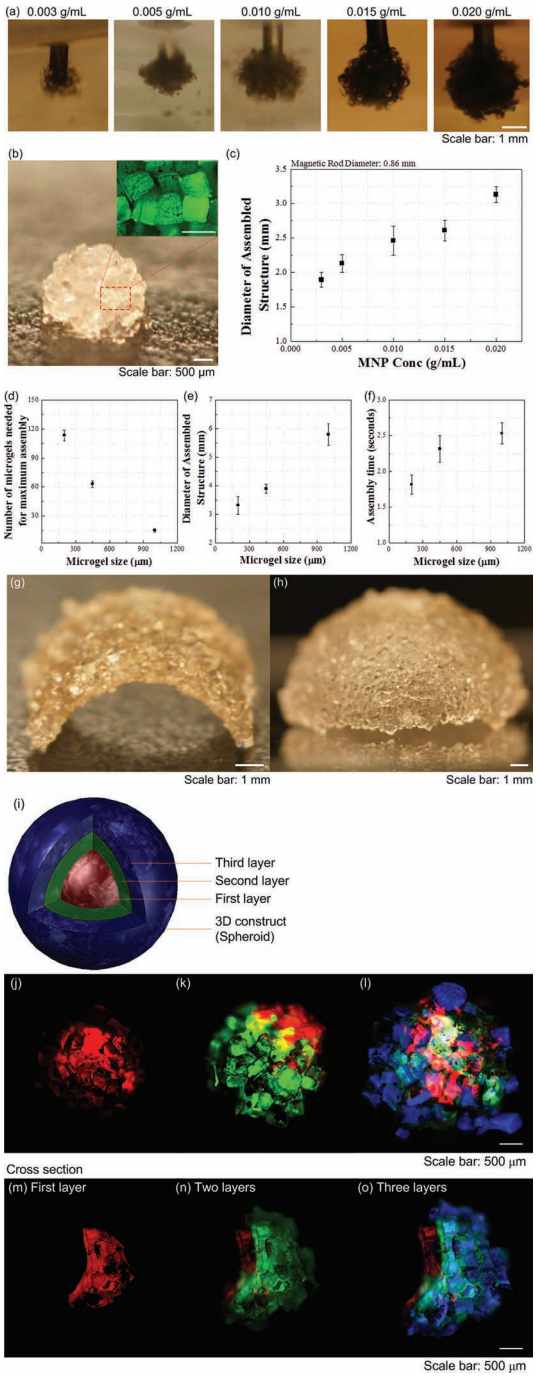


**Figure 4.** Multilayer spherical assembly of M-gels. a) Images of assembled single-layer spheroids using five different MNP concentrations (0.003, 0.005, 0.010, 0.015, and 0.020 g $mL^{-1}$). b) Magnified image of the assembled single-layer 3D construct. c) Maximum 3D assembly size as a function of MNP concentration. The effect of microgel size on d) the number of microgels needed to achieve a maximum assembly size, e) diameter of assembled structure, and f) corresponding assembly time. g,h) Images of fabricated arc and dome-shaped constructs using a flexible surface and magnetic assembly. i–o) Merged fluorescent images of three-layer spheroids. First layer gels were stained with rhodamine-B (j); second layer gels were stained with FITC-dextran (k); third layer gels were stained with TPB (1,1,4,4-tetraphenyl-1,3-butadiene) (l). m–o) The cross sections of the layers obtained by cutting the assembled construct into two hemispheres. The images were merged showing all three layers.

control to a specified location in three dimensions. Furthermore, the existing methods have shown assembly mostly in two dimensions where gels come together randomly. Here, we present assembly in three dimensions where microgels are not only assembling side-by-side but around a field in all directions controlled by the magnetic field strength and interference. Although the earlier work on microgel assembly in two dimensions is intriguing, these assembled gels are now larger in size and need to further be assembled to build even larger and physiologically relevant complex structures that could be useful for tissue engineering applications. To build such larger constructs, the scalability of the assembly mechanisms of existing methods has not been demonstrated. The magnetic assembly method presents a large scale assembly with control over multiple layers of gels rapidly by using a simplistic approach, where existing assembly methods mostly have not gone beyond the assembly of few gels next to each other in 2D repeatably. For instance, the magnetic method can create multilamellar (i.e., multilayer) 3D constructs of complex shapes repeatably using the same MNP concentration levels, and assemble different layer thicknesses by changing these concentrations. The magnetic manipulation of M-gels into microarrays poses a scalable method, as indicated by the above results on chamber sizes, assembly times, and distribution of gel numbers. Although we only presented up to an $8 \times 8$ array formation in this study, the method is shown to be scalable without significantly increasing assembly times. We envision that for a large-scale process, the $8 \times 8$ microarray contained within an area of 5 cm $\times$ 5 cm can be placed into microfluidic systems merged with the proposed magnetic assembly approach. The combination would enable a small array (i.e., $8 \times 8$ array) to be assembled, screened, and dispersed quickly. In this sense, the magnetic-driven assembly is a major step beyond the existing assembly methods and is a unique approach to tissue assembly.

It is important to notice that there are also limitations on the maximum amplitude for the local magnetic field for the 3D assembly. High levels of magnetic force may shear the gels and can influence the microgel integrity. In this study, low intensity magnetic fields yielded assembly of these MNP encapsulating microgels. There are limitations on the amplitude and duration of the magnetic fields that can be used. The use of alternating current (AC)-based magnetic fields may lead to a certain amount of heat (magnetic hyperthermia) that may counter-act the process of magnetic assembly. Since the assembly was performed in several seconds using permanent magnets, we did not observe such adverse affects, however, these design parameters need to be considered for larger scale constructs. We also expect that the shape of the microgels will affect the assembly process, where more complex shapes such as saw and lock-key actually makes it harder to assemble these gels in controlled geometries. Since agglomeration of MNPs is known to occur in prepolymer solutions,[62,63] there exists a possibility that the MNP distribution is not the same in each M-gel. Thus, some M-gels could have a lower affinity to the magnetic field. Hence, prefiltering and sonication of MNPs could minimize non-uniformities from the process steps. Another challenge with this method is that some of the M-gels did not remain on the chamber floor, but floated to the surface of the PBS, which can be solved by adding more PBS to


© 2011 WILEY-VCH Verlag GmbH & Co. KGaA, Weinheim

settle these floating M-gels. Another solution is using microfluidic channels to refrain from such challenges that may be related to the surface tension of the fluids that the gels reside in during assembly.

This study indicates that the developed methodology can potentially become a complementary and simpler surrogate for engineering multilayer 3D constructs. The magnetic assembler reported here has the potential to impact on multiple fields including tissue engineering and regenerative medicine, pharmacology, and stem cell research.

## Supporting Information

Supporting Information is available from the Wiley Online Library or from the author.

## Acknowledgements

This work was performed at the Demirci Bio-Acoustic MEMS in Medicine (BAMM) Laboratories at the Harvard-Massachusetts Institute of Technology Health Sciences and Technology (HST), Center for Bioengineering at Brigham and Women's Hospital, Harvard Medical School. The authors thank Imran Khimji for helpful discussions. This work was partially supported by NIH R21 (EB007707). We thank the MIT Deshpande Center Award, W.H. Coulter Foundation Young Investigator Award, NIH R01 (AI081534), NIH R21 (AI087107), and Integration of Medicine and Innovative Technology (CIMIT) under U.S. Army Medical Research Acquisition Activity Cooperative Agreement, as well as made possible by a research grant that was awarded and administered by the U.S. Army Medical Research & Materiel Command (USAMRMC) and the Telemedicine & Advanced Technology Research Center (TATRC), at Fort Detrick, MD.

Received: May 26, 2011
Revised: June 13, 2011
Published online: August 10, 2011

[1] J. W. Nichol, A. Khademhosseini, *Soft Matter* **2009**, *5*, 1312.
[2] R. Perez-Castillejos, *Mater. Today* **2010**, *13*, 32.
[3] R. Langer, J. P. Vacanti, *Science* **1993**, *260*, 920.
[4] R. J. Davenport, *Science* **2005**, *309*, 84.
[5] L. G. Griffith, M. A. Swartz, *Nat. Rev.* **2006**, *7*, 211.
[6] Y. S. Song, R. L. Lin, G. Montesano, N. G. Durmus, G. Lee, S. S. Yoo, E. Kayaalp, E. Haeggstrom, A. Khademhosseini, U. Demirci, *Anal. Bioanal. Chem.* **2009**, *395*, 185.
[7] F. Xu, J. Celli, I. Rizvi, S. Moon, T. Hasan, U. Demirci, *Biotechnol. J.* **2011**, *6*, 204.
[8] K. M. Yamada, E. Cukierman, *Cell* **2007**, *130*, 601.
[9] D. W. Hutmacher, *Nat. Mater.* **2010**, *9*, 90.
[10] G. R. Souza, J. R. Molina, R. M. Raphael, M. G. Ozawa, D. J. Stark, C. S. Levin, L. F. Bronk, J. S. Ananta, J. Mandelin, M. M. Georgescu, J. A. Bankson, J. G. Gelovani, T. C. Killian, W. Arap, R. Pasqualini, *Nat. Nanotechnol.* **2010**, *5*, 291.
[11] F. Xu, S. Moon, A. E. Emre, E. S. Turali, Y. S. Song, A. Hacking, Nagatomi, U. Demirci, *Biofabrication* **2010**, *2*, 014105.
[12] Y. Du, E. Lo, S. Ali, A. Khademhosseini, *Proc. Natl. Acad. Sci. USA* **2008**, *105*, 9522.
[13] S. Moon, S. K. Hasan, Y. S. Song, F. Xu, H. O. Keles, F. Manzur, S. Mikkilineni, J. W. Hong, J. Nagatomi, E. Haeggstrom, A. Khademhosseini, U. Demirci, *Tissue Eng. Part C* **2010**, *16*, 157.
[14] A. P. McGuigan, B. Leung, M. V. Sefton, *Nat. Protoc.* **2006**, *1*, 2963.
[15] V. Liu Tsang, A. A. Chen, L. M. Cho, K. D. Jadin, R. L. Sah, S. DeLong, J. L. West, S. N. Bhatia, *FASEB J.* **2007**, *21*, 790.
[16] B. Zamanian, M. Masaeli, J. W. Nichol, M. Khabiry, M. J. Hancock, H. Bae, A. Khademhosseini, *Small* **2010**, *6*, 937.
[17] A. Abbott, *Nature* **2003**, *424*, 870.
[18] F. Pampaloni, E. G. Reynaud, E. H. K. Stelzer, *Nat. Rev.* **2007**, *8*, 839.
[19] S. J. Bryant, J. L. Cuy, K. D. Hauch, B. D. Ratner, *Biomaterials* **2007**, *28*, 2978.
[20] M. S. Hahn, L. J. Taite, J. J. Moon, M. C. Rowland, K. A. Ruffino, J. L. West, *Biomaterials* **2006**, *27*, 2519.
[21] S. H. Lee, J. J. Moon, J. L. West, *Biomaterials* **2008**, *29*, 2962.
[22] E. Mercey, P. Obeid, D. Glaise, M. L. Calvo-Munoz, C. Guguen-Guillouzo, B. Fouque, *Biomaterials* **2010**, *31*, 3156.
[23] N. Bassik, B. T. Abebe, K. E. Laflin, D. H. Gracias, *Polymer* **2010**, *51*, 6093.
[24] A. R. Kose, B. Fischer, L. Mao, H. Koser, *Proc. Natl. Acad. Sci. USA* **2009**, *106*, 21478.
[25] M. D. Krebs, R. M. Erb, B. B. Yellen, B. Samanta, A. Bajaj, V. M. Rotello, E. Alsberg, *Nano. Lett.* **2009**, *9*, 1812.
[26] G. Frasca, F. Gazeau, C. Wilhelm, *Langmuir* **2009**, *25*, 2348.
[27] B. B. Yellen, O. Hovorka, G. Friedman, *Proc. Natl. Acad. Sci. USA* **2005**, *102*, 8860.
[28] C.-H. Chen, A. R. Abate, D. Lee, E. M. Terentjev, D. A. Weitz, *Adv. Mater.* **2009**, *21*, 3201.
[29] Q. Pankhurst, J. Connolly, S. K. Jones, J. Dobson, *J. Phys. D* **2003**, *36*, R167.
[30] E. Alsberg, E. Feinstein, M. P. Joy, M. Prentiss, D. E. Ingber, *Tissue Eng.* **2006**, *12*, 3247.
[31] P. E. Le Renard, O. Jordan, A. Faes, A. Petri-Fink, H. Hofmann, D. Rufenacht, F. Bosman, F. Buchegger, E. Doelker, *Biomaterials* **2010**, *31*, 691.
[32] C. B. Coleman, R. A. Gonzalez-Villalobos, P. L. Allen, K. Johanson, K. Guevorkian, J. M. Valles, T. G. Hammond, *Biotechnol. Bioeng.* **2007**, *98*, 854.
[33] J. Dobson, *Nat. Nanotechnol.* **2008**, *3*, 139.
[34] A. Ito, K. Ino, T. Kobayashi, H. Honda, *Biomaterials* **2005**, *26*, 6185.
[35] H. Akiyama, A. Ito, Y. Kawabe, M. Kamihira, *Biomedical Microdevices* **2009**, *11*, 713.
[36] M. Okochi, S. Takano, Y. Isaji, T. Senga, M. Hamaguchi, H. Honda, *Lab Chip* **2009**, *9*, 3378.
[37] C. J. Meyer, F. J. Alenghat, P. Rim, J. H.-J. Fong, B. Fabry, D. E. Ingber, *Nat. Cell. Biol.* **2000**, *2*, 666.
[38] D. K. Hwang, D. Dendukuri, P. S. Doyle, *Lab Chip* **2008**, *8*, 1640.
[39] D. C. Pregibon, M. Toner, P. S. Doyle, *Langmuir* **2006**, *22*, 5122.
[40] K. P. Yuet, D. K. Hwang, R. Haghgooie, P. S. Doyle, *Langmuir* **2009**.
[41] H. Lee, J. Kim, H. Kim, S. Kwon, *Nat. Mater.* **2010**, *9*, 745.
[42] K. W. Bong, S. C. Chapin, P. S. Doyle, *Langmuir* **2010**, *26*, 8008.
[43] J. A. Burdick, K. S. Anseth, *Biomaterials* **2002**, *23*, 4315.
[44] C. R. Nuttelman, M. C. Tripodi, K. S. Anseth, *J. Biomed. Mater. Res.* **2004**, *68*, 773.
[45] S. I. Fraley, Y. Feng, R. Krishnamurthy, D. H. Kim, A. Celedon, G. D. Longmore, D. Wirtz, *Nat. Cell. Biol.* **2010**, *12*, 598.
[46] M. H. Zaman, L. M. Trapani, A. L. Sieminski, D. MacKellar, H. Gong, R. D. Kamm, A. Wells, D. A. Lauffenburger, P. Matsudaira, *Proc. Natl. Acad. Sci. USA* **2006**, *103*, 10889.
[47] Y. Luo, M. S. Shoichet, *Nat. Mater.* **2004**, *3*, 249.
[48] H. Geckil, F. Xu, X. Zhang, S. Moon, U. Demirci, *Nanomedicine* **2010**, *5*, 469.
[49] D. S. Benoit, M. P. Schwartz, A. R. Durney, K. S. Anseth, *Nat. Mater.* **2008**, *7*, 816.
[50] A. M. Kloxin, M. W. Tibbitt, K. S. Anseth, *Nat. Protoc.* **2010**, *5*, 1867.
[51] A. M. Kloxin, A. M. Kasko, C. N. Salinas, K. S. Anseth, *Science* **2009**, *324*, 59.
[52] P. Friedl, K. Wolf, *Nat. Rev. Cancer* **2003**, *3*, 362.


© 2011 WILEY-VCH Verlag GmbH & Co. KGaA, Weinheim

[53] G. R. Souza, D. R. Christianson, F. I. Staquicini, M. G. Ozawa, E. Y. Snyder, R. L. Sidman, J. H. Miller, W. Arap, R. Pasqualini, *Proc. Natl. Acad. Sci. USA* **2006**, *103*, 1215.
[54] G. R. Souza, E. Yonel-Gumruk, D. Fan, J. Easley, R. Rangel, L. Guzman-Rojas, J. H. Miller, W. Arap, R. Pasqualini, *PLoS One* **2008**, *3*, e2242.
[55] L. LaConte, N. Nitin, G. Bao, *Mater. Today* **2005**, *8*, 32.
[56] D. Hautot, Q. A. Pankhurst, C. M. Morris, A. Curtis, J. Burn, J. Dobson, *Biochim. Biophys. Acta* **2007**, *1772*, 21.
[57] A. G. Mikos, *Tissue Eng.* **2006**, *12*, 3307.
[58] N. W. Choi, M. Cabodi, B. Held, J. P. Gleghorn, L. J. Bonassar, A. D. Stroock, *Nat. Mater.* **2007**, *6*, 908.
[59] S. J. Hollister, *Nat. Mater.* **2005**, *4*, 518.
[60] B. J. Nelson, I. K. Kaliakatsos, J. J. Abbott, *Annu. Rev. Biomed. Eng.* **2010**, *12*, 55.
[61] J. G. Fernandez, A. Khademhosseini, *Adv. Mater.* **2010**, *22*, 2538.
[62] Y. Wang, B. Li, Y. Zhou, D. Jia, *Polym. Adv. Technol.* **2008**, *19*, 1256.
[63] H.-B. Xia, J. Yi, P.-S. Foo, B. Liu, *Chem. Mater.* **2007**, *19*, 4087.


© 2011 WILEY-VCH Verlag GmbH & Co. KGaA, Weinheim

Copyright WILEY-VCH Verlag GmbH & Co. KGaA, 69469 Weinheim, Germany, 2011

ADVANCED MATERIALS

# Supporting Information

for *Adv. Mater.*, DOI: 10.1002/adma.201101962

# Three-Dimensional Magnetic Assembly of Microscale Hydrogels

*Feng Xu , Chung-an Max Wu , Venkatakrishnan Rengarajan , Thomas Dylan Finley , Hasan Onur Keles , Yuree Sung , Baoqiang Li , Umut Atakan Gurkan , and Utkan Demirci **

Submitted to ADVANCED MATERIALS

DOI: 10.1002/adma.201101962

**Supporting Information**

**Three-Dimensional Magnetic Assembly of Microscale Hydrogels**

By *Feng Xu, Chung-an Max Wu, Venkatakrishnan Rengarajan, Thomas Dylan Finley, Hasan Onur Keles, Yuree Sung, Baoqiang Li, Umut Atakan Gurkan* and *Utkan Demirci**

[*] Dr. U. Demirci, Dr. F. Xu, Mr. C.M. Wu, Mr. V. Rengarajan, Mr. T.D. Finley, Mr. H. O. Keles, Ms. Y. Sung, Dr. B. Li, Dr. U.A. Gurkan
Demirci Bio-Acoustic-MEMS in Medicine (BAMM) Laboratory
Center for Biomedical Engineering
Department of Medicine, Brigham and Women's Hospital
Harvard Medical School
Boston, MA (USA)
Email: udemirci@rics.bwh.harvard.edu

Dr. Utkan Demirci
Harvard-MIT Division of Health Sciences and Technology
Massachusetts Institute of Technology
Brigham and Women's Hospital, Harvard Medical School
Cambridge, MA (USA)

| | |
|---|---|
| **Video S1** | This movie shows the assembly process of a line geometry. |
| **Video S2** | This movie shows the process of multi-layer spheroid assembly. |

## S.1. Experimental Methods

**Fabrication of M-gels.** Micromolding method was used to fabricate microgels in this study, **Figure 1a**. We used two types of hydrogels, *i.e.*, poly(ethylene glycol) dimethacrylate (PEG) and gelatin methacrylate (GelMA) hydrogels. PEG hydrogels were used for tests without cells, while GelMA hydrogels were used for cell encapsulation tests in view of its better biocompatibility. PEG precursor solution was prepared by dissolving (40%, wt/wt) PEGMA (MW 1000; Sigma), 2-hydroxy-1-(4-(hydroxyethoxy) phenyl)-2-methyl-1-propanone photoinitiator (1%, wt/wt, Irgacure 2959; CIBA Chemicals), and varying concentrations (0 - 0.02 g $mL^{-1}$) of dry iron(II,III) oxide nanopowder (<50 nm; Sigma-Aldrich) in Phosphate Buffered Saline (PBS). To prepare

GelMA precursor solution, gelatin methacrylate (5%, wt/wt) and photo-initiating powder (1%, wt/wt) were mixed in PBS. PDMS molds were plasma treated to render the surface hydrophilic, after which gel precursor solution was pipetted into the PDMS mold. Air bubbles were removed by agitating the surface with the pipette tip, and the mold was then covered with a glass slide coated with 3-trimethoxysilyl propyl methacrylate (3-TMSPMA; Sigma-Aldrich). Microgels were formed by exposing the gel precursor solution to UV light (2.5 mW $cm^{-2}$) for 30 seconds, removed by gently scraping off the glass surface with a scalpel and collected in PBS. In this study, we used three microgel size: 200 x 200 x 200 μm, 450 x 450 x 450 μm, and 1 x 1 x 1 mm.

**Magnetic assembly of microgels (line geometry in multiple rows).** A chamber for holding gels was constructed by sandwiching alternating layers of 200 μm thick plastic and 50 μm thick double-sided adhesive (DSA) (both 50 x 50 mm, with an inner cutout of dimensions 25 x 25 mm) between two plates of PMMA (50 x 50 x 2 mm), **Figures 1b, S2**. The chamber size (25 x 25 x 0.8 mm) was achieved with three layers of plastic and four layers of adhesive. Two holes were cut on the top PMMA plate using a laser cutter (VersaLaser™, Scottsdale AZ) to serve as inlet/outlet ports. M-gels suspended in PBS (500 μl, 230±10 gels $mL^{-1}$) were pipetted into the chamber, after which the ports were sealed with adhesive. The sheet-shape neodymium magnets (50.8x12.7x1.59 mm, K&J Magnetics) were placed against the PMMA and the resulting assembled gel constructs were analyzed.

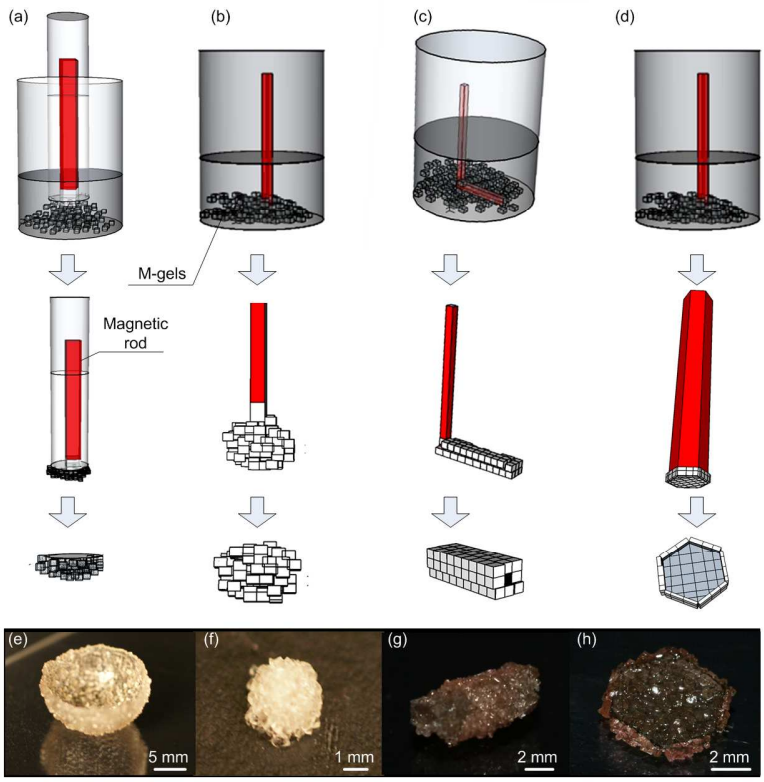


Figure S1. Schematics describing magnetic assembly of 3D structures: (d, h) dome, (e, i) sphere, (f, j) tube, (g, k) hexagon. These geometries were chosen as examples to mimic structures observed *in vivo*, *e.g.*, dome for diaphragm (dome-shaped muscle) beneath the lungs, tube for vascular structure, sphere for islets, hexagon for lobule in pancreas.

**Array formation.** The array formation was developed by magnetically manipulating the M-gels suspended in PBS into separate groups in a chamber made of poly(methyl methacrylate) (PMMA). Neodymium magnets (50.8 mm x 12.7 mm x 1.59 mm; K&J Magnetics) were arranged face-to-face with dielectric spacers, and placed under the chamber bottom to manipulate the scattered M-gels to a row formation (**Fig. 1b**). The magnets were removed from the chamber, rotated by 90 degrees, and reapplied to the chamber to re-manipulate the M-gels from the row

formation into an array formation (**Fig. 1b**) leading to assembled 3D M-gel aggregates in each array element location. The open chamber (1.5 mm in height) was constructed by securing two PMMA sheets (1.5 mm thick) together with a optically clear laminating adhesive sheet (50 µm thick, DSA, 3M 8142) following the laser micromachining methods described in our previous works [1]. The chamber size was designed according to the array size. For instance, the dimensions of the chamber that contained 2x2 and 4x4 microarrays were 25 mm x 25 mm x 1.5 mm, and the chamber dimensions for the 6x6 and 8x8 microarrays were 50 mm x 50 mm x 1.5 mm. The images were captured by a digital camera (Sony α700) and a camcorder (Panasonic HDC-HS9) for videos. To enhance the visibility of the M-gels in the PBS, the prepolymer solution was stained with red food dye.

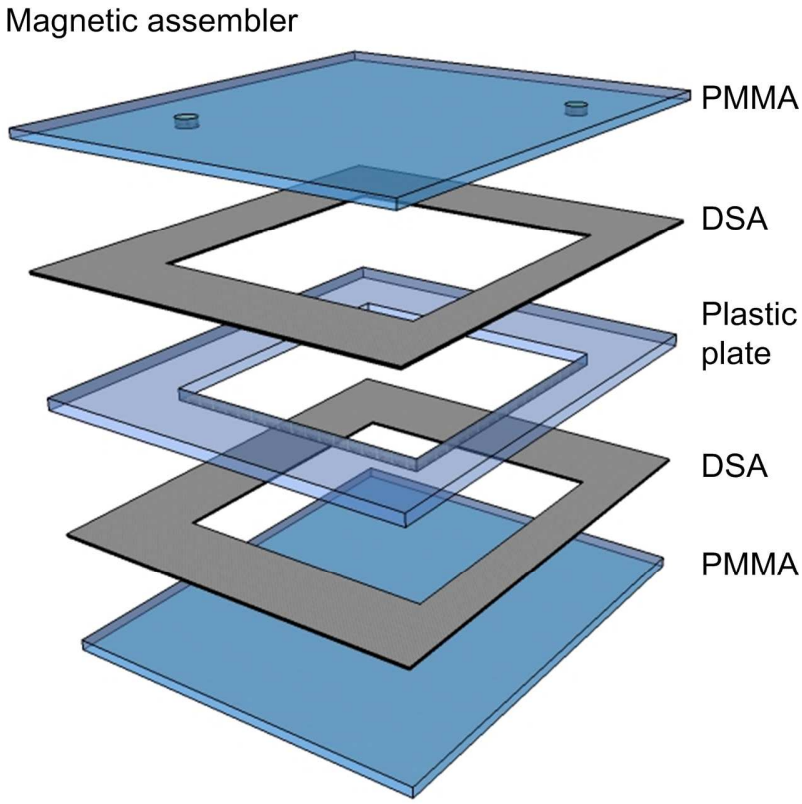


Figure S2. Fabrication and image of a magnetic assembler. The designed magnetic assembler is composed of a fluidic chamber, magnets (50 x 13 x 1.6 mm) and PMMA sheets (2 mm thick) as spacers.

**Measurement of assembly time and quantification of microgel number in each element.** To measure the time duration that takes to assemble arrays of microgels, the fabricated M-gels were suspended in PBS in the open chamber. Then, they were assembled following the process described above utilizing magnets in 90 degrees orientation. We recorded the time needed for each assembly using a stopwatch (Fisher Scientific). This was repeated 10 times for each array size. After each array formation, the array was imaged and the number of gels in each element of

the array was manually counted. The number of gels in each element of the microarray was recorded for statistical analysis.

**Magnetic assembly of microgels (spheroids).** The assembly of spheroid was performed as described in **Figure 1c**. M-gels were collected in PBS in vials (2 mL). To assemble a single type of gel into a spheroid, a magnetized rod was used by attaching an iron paper clip to permanent neodymium magnets (25.4 mm in diameter and 4.76 mm in thickness, K&J Magnetics). To collect the M-gels, the rod was held within a centimeter from the gels to so that the distance between rod and gels is shorter than the maximum collection radius. To assemble two layers, gels with two different MNP concentrations were prepared. The inner layer was assembled from gels with the lower MNP concentration, then carried with the magnetized rod into the second gel suspension with higher MNP concentration, where the aforementioned assembly process was repeated to form the secondary outer layer.

**Magnetic assembly of microgels (flexible surface assembly).** Complex 3D structures including a dome, sphere, tube and hexagon were fabricated by spatially assembling the M-gels onto templates using magnetic manipulation, **Figure S1**. The M-gels were attracted to the templates by attaching a neodymium magnet (50.8 mm x 12.7 mm x 1.59 mm; K&J Magnetics) to one end of a ferrous rod to magnetize it.

**Dome**. The magnetized rod was placed inside the curved glass template and the M-gels were attracted to the surface and assembled as a 3D dome structure (**Fig. S1a**). Prepolymer solution (5

μL) was added and crosslinked to stabilize the structure. The assembled construct was removed slowly with a sterile scalpel without breaking the surface of the gels.

**Tube.** We used a magnetized rod with an "L" shape to achieve the tubular structure (**Fig. S1c**). One end of the rod was connected to the magnet while the other end was located near M-gels with low MNP concentration (0.5%). M-gels were attracted toward the whole area of the bent side of the magnetized rod. The first tubular layer was stabilized by secondary crosslinking with prepolymer solution (5 μL). The first layer was then exposed to M-gels with a higher MNP concentration (2%). The second layer of M-gels was assembled on top of the first layer and was stabilized to form a double layer tubular structure.

**Hexagon shape.** One end of a hexagonal rod (Allen Key, 3.74 $cm^2$ cross-sectional area) was connected to the magnet while the other was positioned near M-gels submerged in PBS (**Fig. S1d**). The M-gels assembled on the base of the magnetized rod were stabilized by secondary crosslinking with prepolymer solution (5 μL). The hexagonal structure was finally scraped off of the rod with a scalpel.

**Stabilization of assembled gel constructs.** Following collection of microgels onto the magnetic tip, prepolymer solution (1 μL) was pipetted onto the spheroid. The prepolymer-encased spheroid was then exposed to UV cross-linking for another 15 seconds. For multi-layer spheroids, each layer was stabilized individually (inner layer stabilized prior to assembly of outer layer) to prevent mixing of the two gel types.

**Encapsulation of cells in M-gels and characterization of cell viability.** NIH-3T3 fibroblasts were used in this study. The cells were cultured in DMEM (Sigma-Aldrich) supplemented with FBS (10%, Gibco) and penicillin-streptomycin (1%, Gibco) at 37 $^{o}$C, in a humidified atmosphere with 5% of $CO_2$. The cells (10 million cells $mL^{-1}$) were suspended in the PEG pre-polymer solution with specified MNP concentrations (0.01 g $ml^{-1}$, 0.05 g $ml^{-1}$), which was then used to fabricate microgels with dimensions of 400 μm x 400 μm x 400 μm using micromolding method following the protocol described above. After encapsulation, cell viability was obtained. Cell-encapsulating M-gels were incubated cells with live/dead dyes for 10 min. The live/dead dyes were prepared by diluting calcein AM (2 mL) and ethidium homodimer-1 (0.5 mL, Molecular Probes, Carlsbad, CA) in DPBS (1 mL). The images were taken using a inverted fluorescent microscope (Nikon TE 2000), and cell viability was characterized by analyzing the images using the public domain NIH ImageJ program (developed at the U.S. National Institutes of Health and available at http://rsb.info.nih.gov/nih-image/) at three time points, *i.e.*, 1 h after preparation of cell-encapsulating microgels and after 1, 3 and 5 days of culture in cell media. The controls were cell-encapsulating microgels without MNPs. Cell growth in M-gels was tracked for 108 hours by imaging every 24 hours using an inverted microscope (Nikon TE2000).

**Statistical analysis.** The experimental results were tested for normal distribution with Anderson-Darling normality test. The number of M-gels in each array element was analyzed statistically with one way analysis of variance (ANOVA) with Tukey post-hoc comparisons for repeated measures (n=10). The uniformity of M-gel distribution in the array elements was statistically assessed with Levene's test for equality of variances for four different array sizes (2x2, 4x4, 6x6, 8x8). Uniformity of the element sizes within the arrays were assessed based on the variance in the

data sets, in which less variance indicated higher uniformity. Statistical significance threshold was set at 0.05 (with $p < 0.05$).

**Theoretical analysis and numerical simulation.** Assuming uniform magnetization within particle volume and a spherical incompressible particle, the instantaneous force ($\vec{F}$) on a magnetic dipole can be given by [2]:

$$\vec{F} = \int_{V_p} \nabla(\vec{M} \cdot \vec{B}_{in}) dV = V_p \nabla(\vec{M} \cdot \vec{B}_{in}) \quad (1)$$

where $\vec{M}$ is magnetization, $\vec{B}_{in}$ is magnetic flux density inside the particle, and $V_p$ is the particle volume. The magnetization of a ferroparticle can be rewritten in terms of the external magnetic field $\vec{H}_{ext}$:

$$\vec{M} = 3\left(\frac{\mu_p - \mu_f}{\mu_p + 2\mu_f}\right)\vec{H}_{ext} \quad (2)$$

where $\mu_p$ and $\mu_f$ are the magnetic permeabilities of particle and surrounding medium, respectively. Approximating $\mu_f$ as $\mu_0$ and expressing $\mu_p$ in terms of volume magnetic susceptibility ($\mu_p = \mu_0(1 + \chi_p)$) simplifies Eq.(2) to:

$$\vec{M} = \left(\frac{3\chi_p}{3+\chi_p}\right)\vec{H}_{ext} \quad (3)$$

To find the internal magnetic field ($\vec{H}_{in}$) and flux density of the particle, we must consider the demagnetization field ($\vec{H}_d$), which for a sphere is $\vec{H}_d = \vec{M}/3$. Given that $\vec{H}_{in} = \vec{H}_{ext} - \vec{H}_d$:

$$\vec{H}_{in} = \left(\frac{3}{3+\chi_p}\right)\vec{H}_{ext} \quad (4)$$

Thus, magnetic force on a ferroparticle is expressed as:

$$\vec{F} = V_p \nabla(\vec{M} \cdot \vec{B}_{in}) = V_p \mu_0 \cdot \nabla\left(\vec{M} \cdot (\vec{H}_{in} + \vec{M})\right) = V_p \mu_0 \cdot \nabla\left(\vec{M} \cdot \vec{H}_{in} + |\vec{M}|^2\right) = V_p \mu_0 \left(\frac{9\chi_p + 9\chi_p{}^2}{9 + 6\chi_p + \chi_p{}^2}\right) \cdot \nabla|\vec{H}_{ext}|^2 \quad (5)$$

Equations (1-5) were solved using a finite element analysis program.

**S.2. Microgel array assembly**

High throughput screening applications often require patterning cell-laden gel constructs in an arrays format (gel microarray). To evaluate the assembly of microgel for microarray formation using magnetic manipulation, we assembled 2x2, 4x4, 6x6, and 8x8 microarrays (**Fig. S3a-h**), and measured the distribution of M-gels throughout the arrays (**Fig. S3i-l**). We further assessed the size uniformity of the assembled M-gel arrays (**Fig. S3m**), and observed that there was no statistically significant difference in the number of M-gels in each element. To evaluate the scalability of the M-gel array assembly process, we statistically analyzed the number of M-gels per element in each of the arrays normalized to expected average number of microgels per element (*i.e.*, total number of microgels divided by the number of elements in the array) (**Fig. S3m**). This analysis did not display a significant variation between arrays of different sizes, which indicates the scalability of the platform presented in this study. Even though the statistical analysis did not indicate significant difference in uniformity between the array elements, we observed higher number of M-gels at the corners and some of the array edges (*e.g.*, **Fig. S3i-l**). The uniformity of M-gel density at the central locations was better, since the magnetic field gradients are more uniform in a large field interference pattern in the central region. The 6x6 array contained an outlier, which can be explained by the initial higher number of M-gels at that position due to the random initial distribution of M-gels in the chamber. To assess the rate of the array assembly process, we measured the assembly time for 2x2, 4x4, 6x6, and 8x8 microarrays formation (**Fig. S3n**). We observed that the assembly time for array formation via magnetic manipulation of M-gels increased with increasing array size from 2x2 to 8x8. It took 27.2 ± 6.0, 32.8 ± 6.5, 43.6 ± 7.7, and 37.2 ± 8.4 seconds to assemble 2x2, 4x4, 6x6, and 8x8 microarrays, respectively. These results indicated that there is a non-linear relationship between the array size and its assembly time.

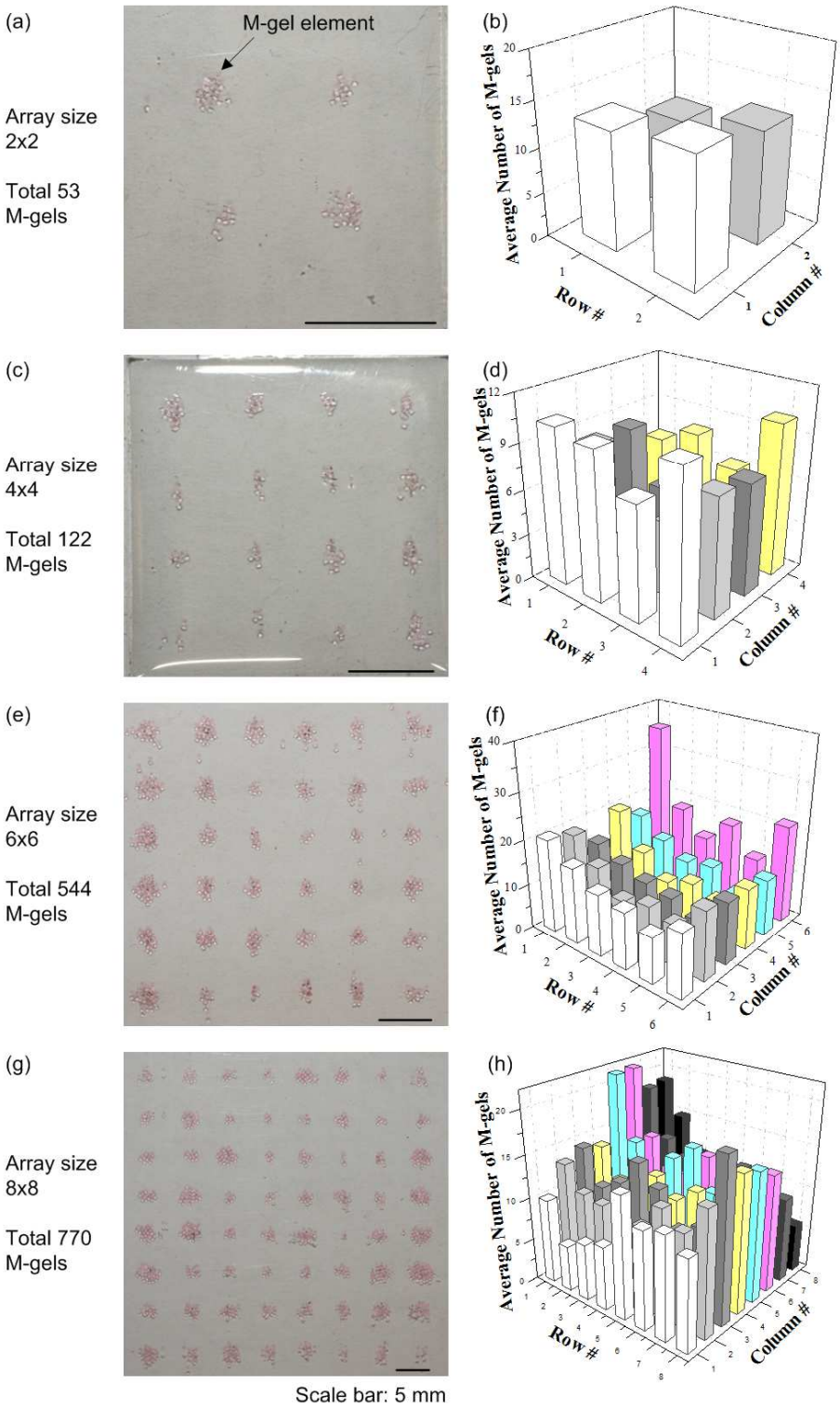
(a)
M-gel element
Array size
2x2
Total 53
M-gels
(b)
Average Number of M-gels
Row #
Column #
(c)
Array size
4x4
Total 122
M-gels
(d)
Average Number of M-gels
Row #
Column #
(e)
Array size
6x6
Total 544
M-gels
(f)
Average Number of M-gels
Row #
Column #
(g)
Array size
8x8
Total 770
M-gels
(h)
Average Number of M-gels
Row #
Column #
Scale bar: 5 mm

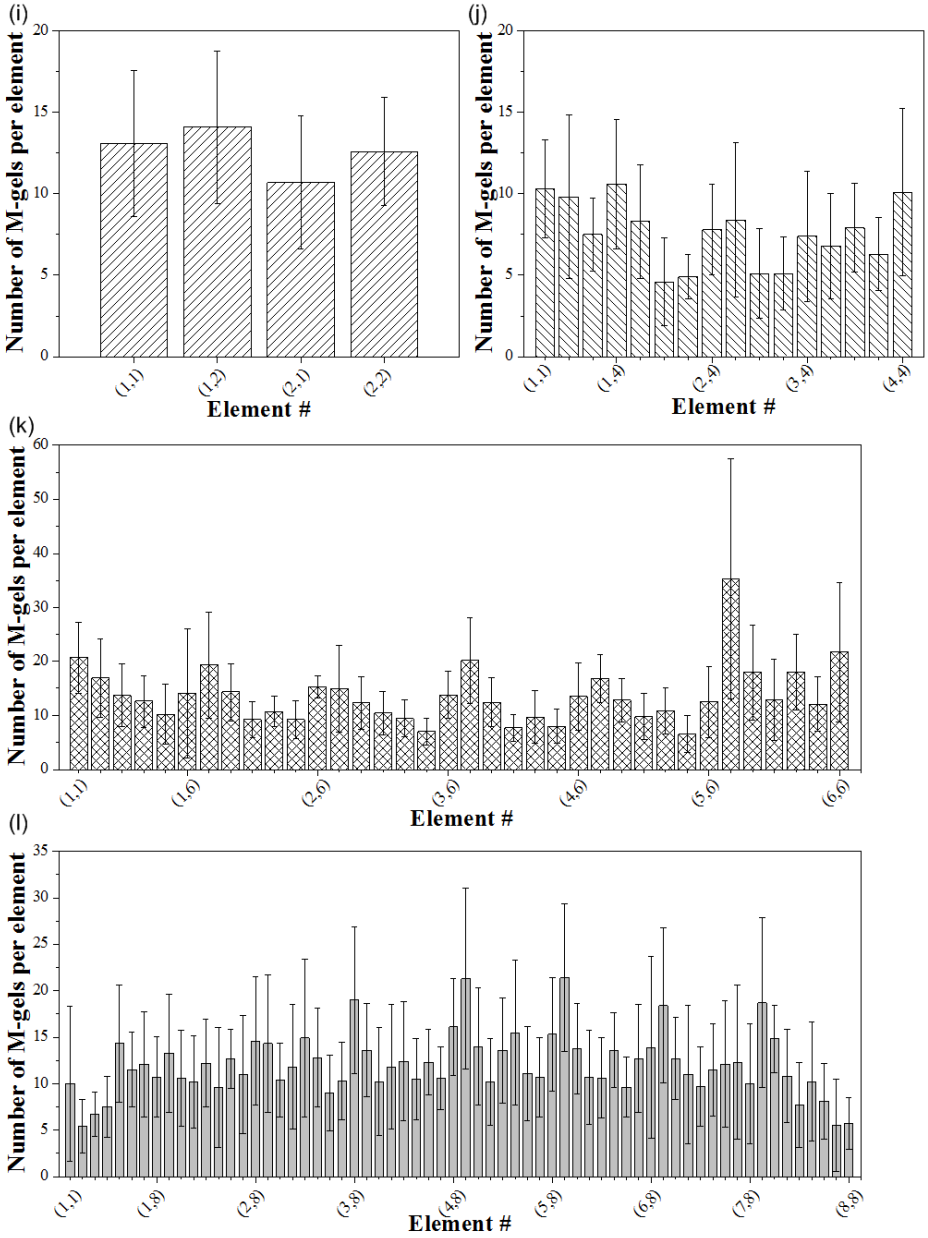
(i)
Number of M-gels per element
Element #
(1,1)
(1,2)
(2,1)
(2,2)
(j)
Number of M-gels per element
Element #
(1,1)
(1,4)
(2,4)
(3,4)
(4,4)
(k)
Number of M-gels per element
Element #
(1,1)
(1,6)
(2,6)
(3,6)
(4,6)
(5,6)
(6,6)
(l)
Number of M-gels per element
Element #
(1,1)
(1,8)
(2,8)
(3,8)
(4,8)
(5,8)
(6,8)
(7,8)
(8,8)

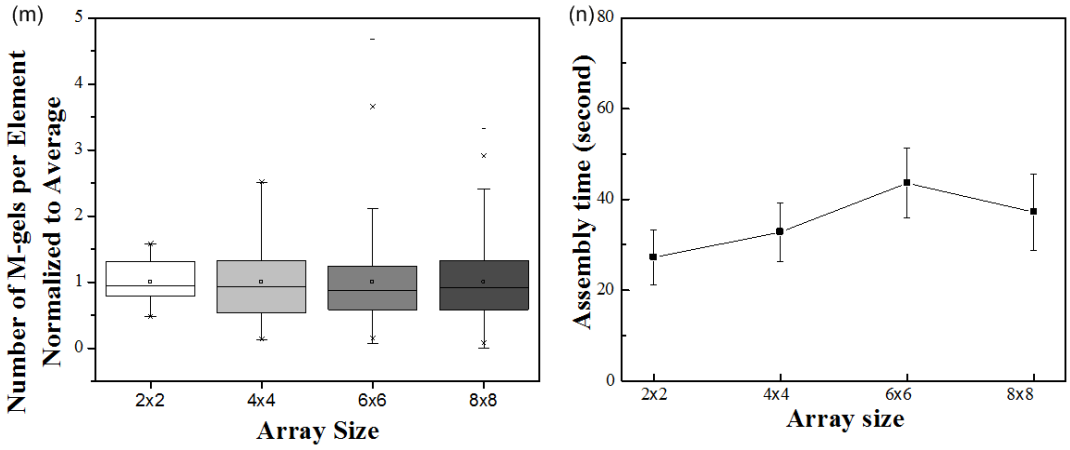


Figure S3. Microarray formation. (a) A 2x2 microarray formed using 53 M-gels, (b) distribution of M-gels in each array element, where elements 1, 2, 3, and 4 were (1,1), (1,2), (2,1), and (2,2), respectively. (c) A 4x4 microarray formed using 122 M-gels, (d) distribution of M-gels in each array element. (e) A 6x6 microarray formed using 544 M-gels, (f) distribution of M-gels in each array element. (g) An 8x8 microarray using 770 M-gels, (h) distribution of M-gels in each array element. Distribution of microgels in arrays of (i) 2x2, (j) 4x4, (k) 6x6, (l) 8x8. (m) Statistical Analysis of M-gel distribution over the array elements. A boxplot showing the number of M-gels per element in each of the arrays normalized to the expected average, *i.e.*, total number of gels divided by the number of array elements. The 2x2 array had the smallest overall range and the smallest interquartile range (IQR). There were several elements with M-gel numbers above the normalized median, and no outliers. The 4x4 array had a large overall range with a high maximum and the largest IQR. The M-gel numbers were evenly balanced around the normalized median. The 6x6 array had a small overall range and a small IQR with M-gel numbers balanced around the normalized median. The 8x8 array had a similar overall range and a smaller IQR compared to the 4x4 array. It had a balance around the normalized median. Even though the 8x8 array contains the second largest IQR, there was not a significant difference compared to the smaller sized arrays. (n) Assembly time to form M-gel arrays with different array sizes. Assembly duration for different size microgel arrays did not display a significant difference with increasing array size.

**References**

[1] S. Moon, H. O. Keles, A. Ozcan, A. Khademhosseini, E. Haeggstrom, D. Kuritzkes, U. Demirci, *Biosensors & bioelectronics* **2009**, *24*, 3208.
[2] M. Zahn, D. R. Greer, *J of Magnetism and Magnetic Materials* **1995**, *149*, 165.